JOURNAL OF SOLID STATE CHEMISTRY 59, 71–80 (1985)

Structure Determination of Ca_2MnO_4 and $Ca_2MnO_{3.5}$ by X-Ray and Neutron Methods

M. E. LEONOWICZ,* K. R. POEPPELMEIER,† AND J. M. LONGO‡

Exxon Research and Engineering Company, Annandale, New Jersey 08801

Received September 28, 1984; in revised form January 11, 1985

The X-ray structure of Ca_2MnO_4 by single crystal analysis and the X-ray and neutron structures of polycrystalline $Ca_2MnO_{3.5}$ by Rietveld analysis have been determined. Ca_2MnO_4 crystallizes in the tetragonal space group $I4_1/acd$ with lattice constants $a = 5.183(1)$ Å and $c = 24.117(4)$ Å, a super-cell ($a = \sqrt{2}a'$, $c = 2c'$) of the $I4/mmm$ unit cell reported from powder diffraction work. This larger unit cell results from rotations of the MnO_6 octahedra about their z axes which produce a Mn–O–Mn bond angle of 161.6° between corner-connected polyhedra. $Ca_2MnO_{3.5}$ crystallizes in the orthorhombic space group $Bbcm$ with lattice constants $a = 5.30$ Å, $b = 10.05$ Å, and $c = 12.23$ Å. The oxygen defects in the structure produce layers of interconnected MnO_5 square-pyramids analogous to those found in the defect perovskite $CaMnO_{2.5}$. The relationship between the $Ca_2MnO_4/Ca_2MnO_{3.5}$ and the $CaMnO_3/CaMnO_{2.5}$ structures is discussed.

Introduction

In a previous paper (*1*) we described the preparation of the compounds $CaMnO_{2.5}$ and $Ca_2MnO_{3.5}$ by low-temperature reduction of $CaMnO_3$ and Ca_2MnO_4. Subsequently, we showed (*2*) that the low-temperature synthesis of the oxygen-deficient compound $CaMnO_{2.5}$ from $CaMnO_{3.0}$ preserves the existing structural framework of the oxidized precursor. This paper describes the synthesis and X-ray structure determination of Ca_2MnO_4 single crystals and the structure determination of polycrystalline $Ca_2MnO_{3.5}$ by both X-ray and neutron Rietveld refinement methods. The essential structural features found in $CaMnO_{2.5}$ (*2*) have now been verified for the $Ca_2MnO_{3.5}$ material. Both compounds show a common distortion of the MnO_6 octahedral frameworks found in the perovskite structure of $CaMnO_3$ and the K_2NiF_4 structure of Ca_2MnO_4, a distortion due to oxygen vacancies generated by the reduction of Mn^{4+} to Mn^{3+}. Thus, the original basis (*1*) upon which the $CaMnO_{2.5}$ model was proposed, namely that the preference of Mn^{+3} for square pyramidal coordination would dictate the structural chemistry in the reduced material, appears to be valid. Furthermore, these results are consistent with a growing literature (*3, 4*) suggesting that the physical and chemical properties of oxygen-deficient compounds of the type ABO_{3-x} and A_2BO_{4-x} are strongly affected by some preferred coordination of B cations adjacent to oxygen vacancies.

* To whom correspondence should be addressed.

† Present address: Department of Chemistry, Northwestern University, Evanston, Ill. 60201.

‡ Present address: Exxon Production Research Co., Houston, Tex. 77001.

0022-4596/85 $3.00

Experimental

Sample Preparation

Single crystals of Ca_2MnO_4 were grown from a flux of calcium chloride saturated with ~7 mole% calcium oxide. The charge of polycrystalline Ca_2MnO_4 had been prepared from the calcite precursor (*5, 6*) $Ca_2Mn(CO_3)_3$ by decomposition at 1000°C for 3 hr in air. The Ca_2MnO_4 was added to the flux mixture in a platinum crucible, heated to 900°C, and held at this temperature for 3 days. The sample was cooled a few degrees per hour through the eutectic of the $CaO–CaCl_2$ system (*7*) to 700°C, and then more rapidly to room temperature. The crystals were separated from the flux by a water wash. Alternatively, crystals of Ca_2MnO_4 can be grown starting with polycrystalline $CaMnO_3$ and a molar equivalent of CaO in a $CaCl_2$ flux saturated with CaO.

Previous work (*1*) with polycrystalline CaMnO and Ca_2MnO_4 had shown that the oxygen-deficient phases $CaMnO_{2.5}$ and $Ca_2MnO_{3.5}$ could be prepared by reduction in dilute hydrogen in the narrow temperature range 300–325°C. As with single crystals of $CaMnO_3$ (*2*), crystals of Ca_2MnO_4 could not be transformed into single crystals of $Ca_2MnO_{3.5}$ with dilute hydrogen at 300°C. Therefore, the present structural study on $Ca_2MnO_{3.5}$ has been limited to polycrystalline samples. Unreacted carbonate precursor was not detected by XRD or infrared analysis of the polycrystalline Ca_2MnO_4 used in this work. The identification of Ca_2MnO_4 by XRD was confirmed by comparison with the cell parameters reported (*8*) in the literature, although the careful examination of the Ca_2MnO_4 single crystals by X-ray diffraction done in this study has revealed a larger unit cell. Cation stoichiometry and oxygen content of both $Ca_2MnO_{4.0}$ and $Ca_2MnO_{3.5}$ were verified by thermogravimetric methods described previously (*1*); their experimentally determined compositions agreed with theoretical compositions to within 1 at.% for oxygen and 0.25 at.% for calcium and manganese.

Ca_2MnO_4—Single Crystal Data Collection and Structure Refinement

Initially, several single crystals of Ca_2MnO_4 were examined using an Enraf–Nonius CAD-4 diffractometer in automatic search mode with graphite-monochromatized Mo$K\bar{\alpha}$ radiation. The reflections located in these experiments were consistent with the unit cell and space group (a' = 3.665(1) Å, c' = 12.061(2) Å, $I4/mmm$, D_{4h}^{17}, No. 139) previously reported in the literature (*8*) for this material. Attempts to refine the literature (*8*) structure (Ca(4*e*): z = 0.3502; Mn(2*a*); 01(4*c*); 02(4*e*): z = 0.1613) with data (341 intensities) collected using this unit cell, however, converged to unacceptably high discrepancy factors (R_1 = 0.080, R_2 = 0.116, 13 variables). The difference Fourier synthesis computed at this point revealed apparent disorder at the O1 site, with significant electron density at ($\pm\delta$, ½, 0) in the xy plane. While subsequent parameterization of this apparent disorder (δ = 0.081) reduced the discrepancy factors (R_1 = 0.026, R_2 = 0.037, 12 variables), a more careful search for diffracted intensities on the automatic diffractometer revealed that the true lattice of this material is a super-cell of the literature values, with $a = \sqrt{2}a'$ and $c = 2c'$. The analysis of the structure was performed using data collected with this larger unit cell at 20°C. The tetragonal $I4/mmm$ A_2BO_4 structure type and monoclinic, orthorhombic, and other tetragonal distortions of it have been the subjects of recent studies (*9, 10*) in the literature.

The crystal data for Ca_2MnO_4 are summarized in Table I. The space group is uniquely defined by systematic absences and the lattice parameter values were derived from least-squares refinement of the centered angles of 25 reflections. Structure factors were derived by the usual formulas

TABLE I

CRYSTALLOGRAPHIC DATA FOR Ca_2MnO_4

Sample size (mm)	0.10 × 0.10 × 0.07
Formula	Ca_2MnO_4
Formula wt. (g/mole)	199.09
Space group	$I4_1/acd$, D_{4h}^{20} No. 142, 2nd setting
Z	8
Density, (calc. g/ml)	4.08
$\mu(mm^{-1})$, Mo$K\bar{\alpha}$ (λ = 0.71073 Å):	7.09
Lattice constants	
a(Å)	5.183(1)
c(Å)	24.117(4)
V(Å^3)	647.9(4)
Data collection	
2θ range	0–120°
Scan type	θ–2θ
Scan rate	Variable, 2–13°, °2θ/min
Scan range	$2\theta(K\alpha_1)$ − 0.9° to $2\theta(K\alpha_2)$ + 0.9°
No. unique data examined	1099
No. data observed, $I \geq 2\sigma(I)$	375
Refinement	
R_1	0.022
R_2	0.030
ESD, unit wt.	0.90
Data/parameters	19.7
No. parameters refined	19
Extinction, g	4.39×10^{-7}

without correction for absorption of X rays because several ψ scans displayed negligible variation in diffracted intensity. Three reflections periodically monitored during the data collection displayed insignificant intensity variations. The model used to begin the structure refinement was obtained by transforming the literature coordinates to the super-cell and then placing the Mn atom at (8*a*). An alternative model that placed the Mn atom in (8*b*) with site symmetry 222 converged at the point where the discrepancy factors were ~15%. All calculations in the single crystal structure determination were performed using the Enraf–Nonius SDP package of programs, an integrated set of crystallographic programs for PDP-11 series computers. The quantity minimized in the least-squares was $\Sigma w(|F_o|-|F_c|)^2$, where $w = \sigma(F_o)^{-2}$, and the form of the extinction correction applied was $(1 + gI_c)^{-1}$. The inclusion of an extinction correction in the final stages of the structure refinement resulted in substantial improvements in the figures-of-merit. The relatively low number of data adjudged observed even at the $2\sigma(I)$ level results from the large 2θ range explored in the data collection. The final difference Fourier synthesis was generally featureless, with peaks of $\sim\frac{1}{2}$ eÅ^{-3} present at several places throughout the unit cell. A listing of $|F_{obs}|$ and $|F_{calc}|$ values is provided as supplementary material.[1] Table II lists the final refined structural parameters and Table III gives derived bond distances and the Mn–O2–Mn bond angle. All bond angles internal to the Mn octahedra are constrained by symmetry to ideal values.

The question arises as to why evidence for the Ca_2MnO_4 super-cell has not been reported in powder diffraction work (*8*) done on this material. The reason may be the complete absence of any reflection in the low angle region of the diffractogram that would necessitate indexing the pattern with a unit cell larger than that previously reported in the literature. This results from the combined effect of the many general systematic absences characteristic of $I4_1/acd$ along with additional extinctions that occur because all atoms in the Ca_2MnO_4 structure lie in special positions in the unit cell. The lowest angle reflections in the powder pattern that cannot be indexed on the literature cell are the (211,213) pair at 39.0 and 40.5° 2θ for Cu$K\alpha$ radiation. Furthermore, the class of *l*-odd reflections in this structure are generally weak, because

[1] See NAPS document No. 04274 for 3 pages of supplementary material. Order from ASIS/NAPS, Microfiche Publications, P.O. Box 3513, Grand Central Station, New York, NY 10163. Remit in advance $4.00 for microfiche copy or for photocopy, $7.75 up to 20 pages plus $.30 for each additional page. All orders must be prepaid. Institutions and organizations may order by purchase order. However, there is a billing and handling charge for this service of $15. Foreign orders add $4.50 for postage and handling, for the first 20 pages, and $2.00 for additional 10 pages of material. Remit $1.50 for postage of any microfiche orders.

TABLE II

FRACTIONAL COORDINATES AND TEMPERATURE FACTORS FOR Ca_2MnO_4

Atom	Site	Symmetry	x	y	z	B_{eqv} (Å^2)
Ca	16*d*	2	0.0	0.25	0.55101(1)	0.565(4)
Mn	8*a*	$\bar{4}$	0.0	0.25	0.375	0.223(2)
O1	16*d*	2	0.0	0.25	0.45559(6)	0.62(2)
O2	16*f*	2	0.2095(4)	$x + 0.25$	0.125	0.53(1)
	β_{11}	β_{22}	β_{33}	β_{12}	β_{13}	β_{23}
Ca	0.0088(1)	0.00313(8)	0.00018(1)	0.0023(3)	0.0	0.0
Mn	0.00164(3)	β_{11}	0.00014(1)	0.0	0.0	0.0
O1	0.0048(3)	0.0094(4)	0.00014(1)	−0.000(1)	0.0	0.0
O2	0.0036(2)	β_{11}	0.00035(2)	0.0029(4)	0.0001(2)	$-\beta_{13}$

Note. Estimated standard deviations in parentheses refer to the last significant digit. The form of the anisotropic thermal parameter is $\exp[-(h^2\beta_{11} + k^2\beta_{22} + l^2\beta_{33} + hk\beta_{12} + hl\beta_{13} + kl\beta_{23})]$.

only the oxygen atom O2 in special position (16*f*) contributes to their intensities. Thus, a few weak peaks at higher angles might have been overlooked in the indexing process and, indeed, careful examination of a Ca_2MnO_4 powder pattern revealed minor deviations from background at the positions of the (211) and (213) reflections; such deviations could easily be dismissed as noise.

TABLE III

STRUCTURAL RESULTS FOR Ca_2MnO_4

Ca–O1 [1*X*][a]	2.301(1) Å[b]
O1 [4*X*]	2.596(1)
O2 [2*X*]	2.354(1)
O2 [2*X*]	2.778(1)
Mn–O1 [2*X*]	1.944(1)
O2 [4*X*]	1.856(2)
O1–O2	2.688(2)
O2–O2	2.625(2)
Mn–O2–Mn	161.6(1)°

[a] Frequency of occurrence as nearest neighbors of the cation.

[b] Estimated standard deviations in parentheses refers to the last significant digit.

$Ca_2MnO_{3.5}$—Powder Data Collection and Structure Refinement

Both neutron and X-ray powder diffraction data were collected on a polycrystalline sample of $Ca_2MnO_{3.5}$. Neutron data were obtained at the Missouri University Research Reactor (MURR) using neutrons with wavelength 1.293 Å incident on a 10-g sample tightly compressed in a sealed vanadium cylinder. The data, collected at room temperature, should be free of magnetic scattering effects, since magnetic susceptibility measurements performed on this material revealed an ordering temperature well below 20°C. Diffraction data were collected by step scanning over an angular range of 5° $\leq 2\theta \leq$ 100° in increments of 0.1° 2θ on a two-axis diffractometer. X-Ray data were collected on the same sample with Cu$K\bar{\alpha}$ radiation using a Philips APD 3600/02 automated powder diffractometer equipped with a graphite diffracted-beam monochromator and a θ-compensating divergence slit mechanism. The sample was tightly packed from the rear of the sample holder and data were collected in the symmetrical reflection mode by step scanning over an angular range of 13° $\leq 2\theta \leq$ 123° in increments of 0.04° 2θ at room temperature.

The diffractogram of $Ca_2MnO_{3.5}$ can be indexed using an orthorhombic unit cell with $a = 5.30$, $b = 10.05$, $c = 12.23$ Å and systematic absences corresponding to the space group *Bbcm* [(0, 0, 0), ($\frac{1}{2}$, 0, $\frac{1}{2}$)+: $\pm(x, y, z)$, $\pm(-x, -y, z)$, $\pm(\frac{1}{2} + x, \frac{1}{2} - y, z)$, $\pm(\frac{1}{2} + x, \frac{1}{2} - y, -z)$], a nonstandard setting of the space group *Cmca* (D_{2h}^{18}, No. 64). The analysis was carried out in *Bbcm* because the structure of $Ca_2MnO_{3.5}$ is intimately related to that of $CaMnO_{2.5}$, which has orthorhombic lattice constants $a = 5.424$, $b = 10.230$, $c = 3.735$ Å and space group *Pbam* (D_{2h}^{9}, No. 55). This choice of space group setting emphasizes the similarity of lattice constants and space symmetry that exists between the two materials, since *Bbcm* also has an *a* glide plane normal to the *b* axis. Thus, starting values for the *x* and *y* coordinates of the $Ca_2MnO_{3.5}$ structural model could be taken directly from those of $CaMnO_{2.5}$; *z* coordinates for the two atoms (Ca and O1) not restricted to the $z = 0$ mirror plane were derived from the corresponding atoms in the fully oxidized material Ca_2MnO_4. Using Wyckoff notation analogous to that used for the standard setting, the initial coordinates for the structural model were as follows: Ca(16*g*): $x \simeq \frac{3}{4}$, $y \simeq \frac{1}{8}$, $z \simeq \frac{1}{8}$; Mn(8*f*): $x \simeq \frac{1}{4}$, $y \simeq \frac{1}{8}$, $z = 0$; O1(16*g*): $x \simeq \frac{1}{4}$, $y \simeq \frac{1}{8}$, $z \simeq \frac{1}{8}$; O2(8*f*): $x \simeq 0$, $y \simeq \frac{1}{4}$, $z = 0$; O3(4*a*): $x = 0$, $y = 0$, $z = 0$. Coordinates (x', y', z') in the standard setting *Cmca* may be obtained from those (x, y, z) in *Bbcm* by the transformation $x' = z$, $y' = x$, $z' = y$.

The structural refinement of both the X-ray and neutron powder data was performed using the Rietveld analysis computer program DBW3.2 provided (*11, 12*) by D. B. Wiles and R. A. Young. The refinement was done in stages, with the atomic coordinates and thermal parameters held fixed in the initial calculations and subsequently allowed to vary only after the scale, background, half-width, and unit cell parameters were close to convergence on their optimum values. These refinements were characterized by reasonably good figures-of-merit (for the neutron data: $R_P = 4.47$, $R_{WP} = 5.80$, $R_{EX} = 3.21$, $R_{WP}/R_{EX} = 1.81$, $R_B = 1.44$; for the X-ray data: $R_P = 12.68$, $R_{WP} = 17.97$, $R_{EX} = 7.72$, $R_{WP}/R_{EX} = 2.33$, $R_B = 5.10$). However, it was clear from an ($I_{OBS} - I_{CALC}$) difference plot that a second phase was present in the sample in substantial amounts. This component was identified (*5*) as the solid solution Ca_2MnO_3 (*13*), which takes the NaCl structure with O in site (4*a*) and (Ca,Mn) disordered in a 2 : 1 ratio in site (4*b*) of space group *Fm*3*m* (O_h^5, No. 225). The X-ray diffractogram provided the most unambiguous evidence for the presence and identification of the second phase in the sample, with the 10% relative peak at 38.3° and the 7% peak at 55.3° identified as the (200) and (220) reflections of Ca_2MnO_3. The (220) reflection was also clearly present in the neutron difference plot.

Incorporation of this second phase into the scattering model with independently varied scale constant, cubic lattice constant, half-width parameters, and atom thermal parameters significantly improved the figures-of-merit of the refinement, as well as the appearance of both the X-ray and neutron difference plots. Figure 1 shows the observed, calculated, and difference X-ray diffraction patterns for the two-phase Rietveld refinement of the $Ca_2MnO_{3.5}$ data and Fig. 2 is an analogous plot of the neutron data. Table IV contains details of both the X-ray and neutron refinements, including figures-of-merit and final values for all parameters varied in the least-squares analyses except the $Ca_2MnO_{3.5}$ position and temperature parameters that are given in Table V and the background polynomial coefficients, 2θ zero point and individual phase scale factors, whose precise values are unimportant to the discussion of the results. Table VI contains bond distances and angles for $Ca_2MnO_{3.5}$ calculated from

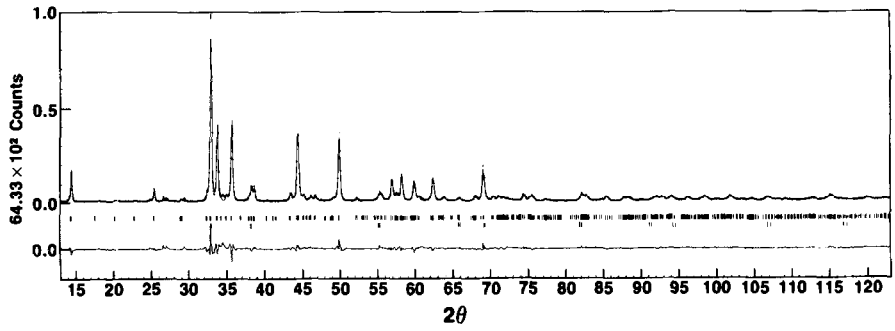

FIG. 1. Observed, calculated, and difference plots of $Ca_2MnO_{3.5}$ X-ray data.

both the X-ray and neutron refinement results.

Careful examination of the $Ca_2MnO_{3.5}$ diffraction patterns reveals that impurities in addition to Ca_2MnO_3 are present in the sample used in these experiments. The evidence is clearer in Fig. 1, where the small peaks observed at ~27, ~29.4, and ~34.5° are not predicted by either phase included in the Rietveld analysis. These peaks may be attributed to minor amounts of impurities because their relative intensities and indeed presence vary between $Ca_2MnO_{3.5}$ preparations. Some can be assigned to byproducts expected in the synthesis. For instance, the peak at 34.5° corresponds to the 75% peak in the standard diffractogram of Ca_2MnO_4 (JCPDS Card No. 24-1194) and its intensity can be used as a measure of the degree to which the starting material has undergone reduction. The Ca_2MnO_4 100% peak at 33° is masked by the intense (123) $Ca_2MnO_{3.5}$ and (111) Ca_2MnO_3 peaks that both occur at ~33°. Similarly, the peak at 29.4° corresponds to the 100% peak in the standard diffractogram for $CaCO_3$ (calcite, JCPDS Card No. 5-586). The one remaining peak at ~27° has not been identified. Differences between the actual instrumental profile function and that used in the Rietveld analysis (*12*) cause sharp peaks in the X-ray difference plot at positions of intense observed reflections. The cause of the high and varying background levels observed in the neutron diffraction pattern is not clear, although similar results were observed in the analogous $CaMnO_{2.5}$ study (*2*). Neither the X-ray nor the neutron Rietveld refinement included any corrections for preferred orientation in the sample, but the X-ray re-

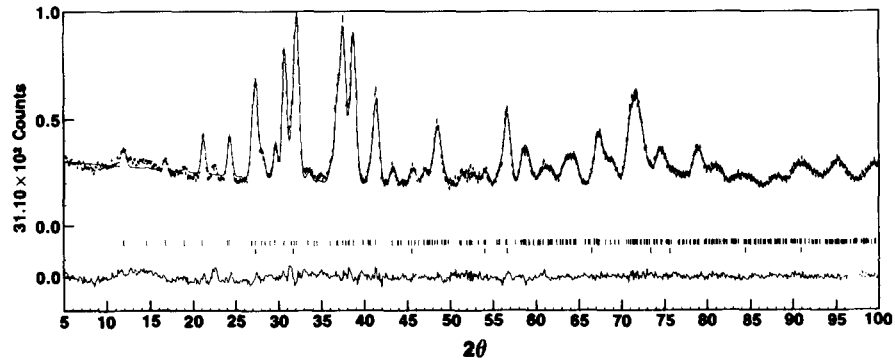

FIG. 2. Observed, calculated, and difference plots of $Ca_2MnO_{3.5}$ neutron data.

TABLE IV
RIETVELD REFINEMENT RESULTS

Figures-of-merit[a]	X-Ray data	Neutron data
R_P	10.66	3.94
R_{WP}	14.61	5.16
R_{EX}	7.71	3.20
R_{WP}/R_{EX}	1.89	1.61
No. of variables	38	36
η	0.83(2)[b]	
	$Ca_2MnO_{3.5}$	
R_B	2.90	1.14
No. of reflections	265	302
a (Å)	5.3029(3)	5.297(1)
b (Å)	10.0540(5)	10.053(2)
c (Å)	12.2300(6)	12.221(2)
U	0.16(2)	2.1(3)
V	−0.04(2)	−0.2(3)
W	0.037(4)	0.31(6)
Asymmetry	0.20(6)	
	Ca_2MnO_3	
R_B	2.40	1.23
No. of reflections	11	11
a (Å)	4.6961(6)	4.704(3)
U	−0.8(3)	−2(3)
V	1.8(3)	4(3)
W	−0.47(7)	−0.6(6)
B(Ca,Mn), Å^2	1.7(3)	6(2)
B(O), Å^2	1.1(5)	1.1(6)

[a] R_p is the profile discrepancy factor, R_{WP} is the weighted profile discrepancy factor and R_{EX} is the expected weighted profile discrepancy factor. R_B is a discrepancy factor based on the difference between observed and calculated integrated intensities; the observed values are obtained by partitioning overlapping peaks in the spectrum. Explicit definitions for the figures-of-merit are given in Refs. (*11, 12*).

[b] Estimated standard deviations in parentheses refer to the last significant digit.

finement (Fig. 1) contains three peaks for which the calculated intensity is markedly lower than that observed. These peaks occur at 33, 50, and 69° 2θ and correspond to the (123), (240), and (246) reflections, respectively. The fact that two members of the (123) family of planes are substantially underestimated may be evidence for a small amount of preferred orientation in the X-ray data, although, as mentioned above, the intensity of the 33° peak is also augmented by the presence of impurities in the sample.

In both the X-ray and neutron data analyses, the background was parameterized as a polynomial function of the diffraction angle 2θ in degrees, where the polynomial coefficients were included in the least-squares refinement. Half-width parameters U, V, and W have their usual meanings and explicit definitions for the figures-of-merit quoted in Table IV, as well as for the asymmetry correction applied to the X-ray profiles, are given in Refs. (*11, 12*). Reflection positions and intensities were calculated for both Cu $K\alpha_1$(λ = 1.5405 Å) and Cu$K\alpha_2$(λ = 1.5443 Å) in the X-ray Rietveld refinement, with a factor of 0.5 applied to the latter's calculated integrated intensities. The profile function used in the neutron data refinement was the usual Gaussian form but the X-ray data was refined using a pseudo-Voigt function (*12*) with the mixing parameter η included in the least-squares refinement. Correction for incident X-ray intensity variation caused by the θ-compensating divergence slit was accomplished by multiplying the calculated integrated intensity of each reflection by a factor $c = \sin(a\theta + b)$, where 2θ in degrees refers to the midpoint of the reflection. Constants a = 0.8438 and b = 6.8140 were determined for a least-squares analysis of the experimentally measured variation of incident intensity with diffraction angle.

Discussion

This work has established that the structural change observed when $CaMnO_3$ is reduced to $CaMnO_{2.5}$ also occurs when Ca_2MnO_4 is reduced to $Ca_2MnO_{3.5}$. Upon reduction in the ABO_3 system (*2*), oxygen sites in the three-dimensional corner-shared network of Mn^{+4} octahedra are defected in planes, thus producing a layer structure of interconnected distorted square-pyramidal Mn^{+3} coordination poly-

TABLE V

FRACTIONAL COORDINATES AND TEMPERATURE FACTORS FOR $Ca_2MnO_{3.5}$

Atom	Site	Symmetry	x	y	z	B (Å^2)
Ca	16*g*	1	0.7862(5)[a,b]	0.1244(7)	0.1521(2)	1.76(7)
			0.7870(12)[c]	0.1251(11)	0.1533(5)	0.88(11)
Mn	8*f*	*m*	0.2672(7)	0.1241(7)	0.0	1.81(9)
			0.2684(26)	0.1304(19)		0.33(17)
O1	16*g*	1	0.2759(15)	0.1193(17)	0.1645(6)	1.85(15)
			0.2718(9)	0.1207(8)	0.1589(4)	0.66(10)
O2	8*f*	*m*	0.0637(26)	0.2960(13)	0.0	1.42(31)
			0.0784(14)	0.2975(8)		1.15(15)
O3	4*a*	2/*m*	0.0	0.0	0.0	1.92(57)
						0.71(21)

[a] Estimated standard deviations in parentheses refer to the last significant digit.
[b] First line of results for each atom gives the final X-ray refinement parameters.
[c] Second line of results for each atom gives the final neutron refinement parameters.

TABLE VI

STRUCTURAL RESULTS FOR $Ca_2MnO_{3.5}$

		X-Ray results	Neutron results
		Distance (Å)	
Ca–O1	$\frac{1}{2}+x, y, \frac{1}{2}-z$	2.24[a]	2.30
O1	$1-x, -y, z$	2.48	2.49
O1	$\frac{1}{2}+x, \frac{1}{2}-y, z$	2.58	2.56
O1	$1+x, y, z$	2.60	2.57
O1	x, y, z	2.71	2.73
Ca–O2	$\frac{1}{2}+x, \frac{1}{2}-y, -z$	2.34	2.31
O2	$1+x, y, z$	2.93	2.98
Ca–O3	$1+x, y, z$	2.51	2.52
Mn–O1	x, y, z	2.01[b]	1.94[c]
O1′	$x, y, -z$	2.01	1.94
Mn–O2	x, y, z	2.04	1.96
O2′	$\frac{1}{2}+x, \frac{1}{2}-y, -z$	1.77	1.80
Mn–O3	x, y, z	1.89	1.93
		Angle (°)	
O1–Mn–O1′		176.2[d]	174.2
O2		91.9	92.7
O2′		89.5	90.7
O3		90.1	88.4
O2–Mn–O2′		94.9	97.1
O3		99.4	101.8
O2′–Mn–O3		165.7	161.1
Mn–O2–Mn		149.0	144.7

[a] The estimated standard deviation of Ca–O bond distances is 0.01 Å.
[b] The estimated standard deviation of Mn–O bond distances is 0.01 Å for the X-ray results.
[c] The estimated standard deviation of Mn–O bond distances is 0.02 Å for the neutron results.
[d] The estimated standard deviation of bond angles is 0.5°.

hedra that retains perovskite-like connectivity in the third direction. The Mn^{+4} octahedra in Ca_2MnO_4 form a perovskite-like network in only two dimensions, with axial oxygens coordinated to Ca atoms in the third direction. Upon reduction, the same defect structure (as illustrated in Figs. 3 and 4 of Ref. (*2*)) is created in the perovskite-like layers of the A_2BO_4 system, with the third direction unaffected. In Fig. 3, the fully oxidized Ca_2MnO_4 structure is contrasted with the defect structure of $Ca_2MnO_{3.5}$; comparison of this figure with Fig. 1 in Ref. (*2*) for the $CaMnO_3/CaMnO_{2.5}$ structures graphically illustrates the similarities between the systems.

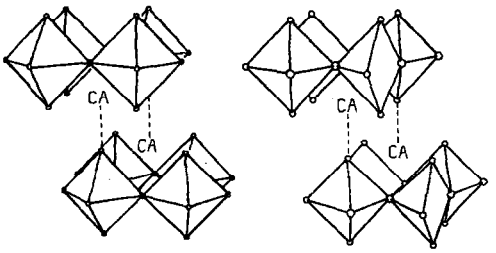

FIG. 3. (a) Fully oxidized MnO_6 sheets in Ca_2MnO_4. (b) Defect MnO_5 sheets in $Ca_2MnO_{3.5}$.

In each example cited above, removal (reduction) of an oxide ion from the lattice generates adjacent Mn^{3+} cations. In these two examples and in other recent examples (largely characterized by electron diffraction (*14*)), corner-connected MnO_5 square-pyramids are the central structural feature of these grossly anion-deficient materials. The original proposal for this coordination was based on the observation that the perovskite-like sheets of octahedral Mn^{4+} found in Ca_2MnO_4 underwent distortion upon reduction in exactly the same fashion as in $CaMnO_3$. That is, the observed unit cell distortion in both $CaMnO_{2.5}$ and $Ca_2MnO_{3.5}$ could be described by the equation $(a_o + b_o/2)/2 = \sqrt{2}a_c$; in this equation, the new orthorhombic unit cell parameters a_o and b_o are related to the distance a_c (~3.7 Å) characteristic of the Mn–O–Mn bond length sum in the oxidized state.

In the analysis of the X-ray and neutron diffraction data of $Ca_2MnO_{3.5}$, the rock-salt phase Ca_2MnO_3 was determined to be the major contaminant. Contamination with this phase was found to be a problem in all preparations of $Ca_2MnO_{3.5}$ when hydrogen was used at reaction temperatures approaching 325°C, and it became the dominant phase at higher temperatures. This is in contrast to the preparation of $CaMnO_{2.5}$ where incomplete reduction (e.g., $CaMnO_{2.75}$) and two-phase decomposition (CaO and $CaMn_2O_4$) reactions were more prevalent. The latter reaction may occur with $Ca_2MnO_{3.5}$, since some CaO (as $CaCO_3$ after exposure to air) was detected, but no evidence could be found for $CaMn_2O_4$. Contamination with minor amounts of other phases is a general concern when reaction conditions are different from those more narrowly defined by equilibrium considerations. The advantage of nonequilibrium reaction conditions lies in that new compounds that are metastable, or perhaps stable only at lower temperatures, can be prepared; however, the concurrent problem of sample homogeneity under these conditions should not be ignored.

The structures of $Ca_2MnO_{3.5}$ determined on the basis of X-ray and neutron data are very similar. Each refinement produces a long Mn–O2 bond length and a relatively short one. This is required since the sum of these two lengths should not differ significantly from 3.7 Å, yet there must be an unequal occupation of the d_{z^2} and $d_{x^2-y^2}$ orbitals by the differentiating electron in $Mn^{3+}(d^4)$. Other manganese–oxygen distances are intermediate in length and follow the same pattern (axial longer than equitorial) found in the oxidized precursor. The magnitudes and distribution of calcium–oxygen bond distances in $Ca_2MnO_{3.5}$ are also similar to those found in Ca_2MnO_4, although the Ca^{2+} coordination number changes from nine to eight upon reduction of the manganese. There are no unusually-short oxygen–oxygen nonbonded contacts in the defect solid; the shortest distance (O1–O2, 2.66 Å) agrees well with the distances found in the oxidized precursor. An important result of the Ca_2MnO_4 structural study is the discovery that the two-dimensional, corner-shared network of MnO_6 coordination polyhedra is distorted by twisting the octahedra by ~9° about their z axes, as shown in Fig. 4. The resulting Mn–O–Mn bond angle (161.6°) is close to those found (*2*) in $CaMnO_3$ (158.6, 157.2°), although the distortion in $CaMnO_3$ results from tilts of the octahedra about all three axes.

As can be seen from the data in Table VI, the X-ray and neutron refinements of $Ca_2MnO_{3.5}$ disagree on several derived bond lengths and angles by more than 3σ. One serious disagreement involves the position of atom O2; a similar discrepancy was found in the $CaMnO_{2.5}$ structure determinations. Others result from a disagreement about the z coordinate of O1. These differences may be due to low error estimates from the Rietveld analysis method

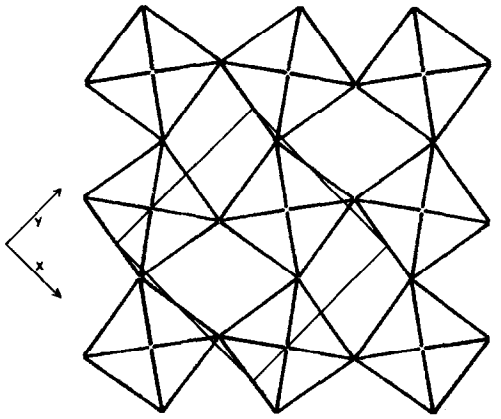

FIG. 4. Orientation of manganese octahedra in Ca_2MnO_4 as viewed from the c direction.

(*15, 16*). Alternatively, if the differences are real, then one might judge the neutron results to be the more reliable from a comparison of figures-of-merit given in Table IV. The neutron data, however, are troubled by the high background levels and broad diffraction peak widths mentioned above. The X-ray diffractogram has a cleaner appearance and there is greater consistency among the thermal parameters derived from this refinement (see Table V), but this analysis will be affected by the inadequacies of the X-ray peak profile function and by the other experimental problems cited earlier. Thus, there are reasons for preferring each set of results, with no clear and unambiguous way to resolve the matter. The neutron data also may be more sensitive to the presence in small amounts of domains with different defect ordering schemes; such domains have been detected in $CaMnO_{2.5}$ by electron diffraction and appear to be associated with the method of preparation (*17*). All the oxygen vacancy order schemes so far proposed for these domains, however, still combine the essential structural features of the starting material with pairs of Mn^{3+} cations in approximately square-pyramidal coordination.

Acknowledgment

The authors express their thanks to Dr. W. B. Yelon for the powder neutron data.

References

1. K. R. POEPPELMEIER, M. E. LEONOWICZ, AND J. M. LONGO, *J. Solid State Chem.* **44,** 89 (1982).
2. K. R. POEPPELMEIER, M. E. LEONOWICZ, J. C. SCANLON, J. M. LONGO, AND W. B. YELON, *J. Solid State Chem.* **45,** 71 (1982).
3. L. ER-RAKHO, C. MICHEL, J. PROVOST, AND B. RAVEAU, *J. Solid State Chem.* **37,** 151 (1981).
4. J. C. GRENIER, M. POUCHARD, AND P. HAGENMULLER, *Struct. Bonding* **47,** 1 (1982).
5. H. S. HOROWITZ AND J. M. LONGO, *Mater. Res. Bull.* **13,** 1359 (1978).
6. K. VIDYASAGER, J. GOPALAKRISHNAN, AND C. N. R. RAO, *Inorg. Chem.* **23,** 1206 (1984).
7. D. A. WENG, I. JOHNSON, AND R. D. WILSON, *J. Chem. Eng. Data* **14,** 252 (1969).
8. J. H. RUDDLESDEN AND P. POPPER, *Acta Crystallogr.* **10,** 538 (1957).
9. P. POIX, *J. Solid State Chem.* **31,** 95 (1980).
10. P. GANGULY AND C. N. R. RAO, *J. Solid State Chem.* **53,** 193 (1984).
11. D. B. WILES AND R. A. YOUNG, *J. Appl. Crystallogr.* **14,** 149 (1981).
12. R. A. YOUNG AND D. B. WILES, *J. Appl. Crystallogr.* **15,** 430 (1982).
13. A. H. JAY AND K. W. ANDREWS, *J. Iron Steel Inst. London* **152,** 15 (1946).
14. A. RELLER, D. A. JEFFERSON, J. M. THOMAS, AND M. K. UPPAL, *J. Phys. Chem.* **87,** 913 (1983).
15. M. SAKATA AND M. J. COOPER, *J. Appl. Crystallogr.* **12,** 554 (1979).
16. H. G. SCOTT, *J. Appl. Crystallogr.* **16,** 159 (1983).
17. A. RELLER, D. A. JEFFERSON, J. M. THOMAS, R. A. BEYERLEIN, AND K. R. POEPPELMEIER, *J. Chem. Soc. Commun.*, 1378 (1982).